actuators

MDPI

Article

Adaptive Time-Varying Formation Maneuvering Control for Multi-Robot Systems in Complex Obstacle-Rich Environments

Junmei Zhao [1,*], Liping Zhang [1], Xiao Li [1], Kewu Li [1], He Wang [2] and Yeye Liu [1]

[1] School of Electrical and Control Engineering, North University of China, Taiyuan 030000, China; zhangliping@nuc.edu.cn (L.Z.); lixiaoydx@nuc.edu.cn (X.L.); kewuli@nuc.edu.cn (K.L.); 20240042@nuc.edu.cn (Y.L.)

[2] College of Intelligent Systems Science and Engineering, Harbin Engineering University, Harbin 150001, China; wang_he@hrbeu.edu.cn

* Correspondence: zhaojunmei@nuc.edu.cn

Abstract: To tackle the challenge of time-varying formation control for underactuated robots under model parameter uncertainties and environmental disturbances, this study proposes an affine formation control approach enhanced by an Extended State Observer. Initially, using affine positioning theory and polynomial interpolation, guidelines for selecting leader vehicles and trajectory planning methods are established, whereby the trajectory of follower vehicles is uniquely determined through the stress matrix. To address the cumulative disturbances arising from model uncertainties and environmental factors impacting the formation, an Extended State Observer with optimized parameters is introduced. Furthermore, a distributed affine formation control method with disturbance rejection is designed specifically for underactuated robots with "nonlinear, strongly coupled" dynamics, ensuring that the formation system can track the target configuration within bounded error margins. Finally, theoretical analysis and simulation outcomes ultimately confirm the efficacy of the control approach in achieving resilient formation tracking.

Keywords: underactuated robots; disturbance rejection; time-varying formation control; affine transformation

check for updates

Citation: Zhao, J.; Zhang, L.; Li, X.; Li, K.; Wang, H.; Liu, Y. Adaptive Time-Varying Formation Maneuvering Control for Multi-Robot Systems in Complex Obstacle-Rich Environments. *Actuators* **2024**, *13*, 493. https://doi.org/10.3390/act13120493

Academic Editors: Iacopo Tamellin and Jason Bettega

Received: 7 November 2024
Revised: 27 November 2024
Accepted: 1 December 2024
Published: 2 December 2024

Copyright: © 2024 by the authors. Licensee MDPI, Basel, Switzerland. This article is an open access article distributed under the terms and conditions of the Creative Commons Attribution (CC BY) license (https://creativecommons.org/licenses/by/4.0/).

1. Introduction

With the swift advancement of robotics and automation, the coordinated operation of multi-robot systems has emerged as a key area of research in intelligent control [1]. Particularly in dynamic tasks performed in complex environments, a single robot often struggles to effectively cover large areas and collect data. In contrast, multi-robot formations can greatly enhance the efficiency and task performance of the system through coordinated cooperation [2]. Time-varying formation control, as a critical method in multi-robot systems, dynamically adjusts the formation of robots to adapt to environmental changes and task requirements, significantly improving the flexibility and adaptability of the system.

To address the complexities of time-varying formation control, researchers have examined a variety of transformation methods founded on three core approaches: displacement, distance, and orientation. For instance, Zelazo et al. enhanced fixed formation control through a displacement-based scaling estimation mechanism [3], while Liu et al. optimized distance-based control by introducing a scaling factor, enabling more adaptable time-varying formation adjustments [4]. Nevertheless, these methods often result in complex control and estimation challenges, requiring additional sensing or communication resources for each agent. Similarly, Alfakih et al. introduced a time-varying formation control technique [5], though it relies on predefined paths for each agent. To overcome these challenges, new methods have been introduced, including local bearing [6], centroid coordinate systems [7], complex Laplacian matrices [8], and stress matrices [9]. These newer approaches address certain limitations of traditional methods and support a range of

formation maneuvers like translation, rotation, and scaling, yet they are not without their own challenges. For example, local bearing and centroid-based controls demand designing relative rotation matrices, while the complex Laplacian matrix approach is better suited for formations of specific dimensions. The stress matrix, seen as an extended form of a Laplacian graph, is defined by the structure of the underlying graph with each element influenced by the formation layout and graph configuration. Unlike standard Laplacian matrices, stress matrix edge weights may be positive, negative, or zero, although stress matrix-based methods are limited to basic formation maneuvers. Affine transformations, on the other hand, provide a broader framework for linear transformations, which are capable of representing translation, rotation, scaling, shearing, and combinations thereof. The stress matrix remains unaffected under any affine transformation of the formation layout, so by combining stress matrices with affine transformations, a wider range of formation maneuvers becomes possible.

The combination of stress matrices and affine transformations has established a foundational framework for exploring time-varying formation generation and control. Lin et al. introduced a new problem in multi-agent systems, called affine formation control, and identified necessary and sufficient conditions based on graph theory for achieving affine formations under both directed and undirected interaction graphs [9]. They also devised a balanced-stress-based control law, providing a robust theoretical base for future research in affine formation control. Zhao advanced this area by designing an efficient formation controller that combines the stress matrix with affine transformations, allowing multi-agent formations to perform maneuvers like translation, rotation, scaling, and shearing. Zhao's work not only broadened the application of affine formation control in various domains but also strengthened the theoretical foundation for cooperative control in multi-agent systems [10]. Pang et al. tackled the nonlinear distributed control challenge in 3D environments by developing a formation reconstruction method based on graph rigidity and affine transformations, specifically for autonomous underwater vehicles (AUVs) in oceanic settings [11]. Meanwhile, Chen et al. proposed a novel 3D maneuver control approach for nonlinear multi-agent systems under nonholonomic constraints, incorporating saturated control in a distributed communication framework that enhances flexibility and effectiveness for routine formation tasks [12]. Zhu et al. investigated a scenario where only the leader receives commands for formation transformation gains, employing affine transformations to define the target formation and designing a combined constraint framework using the stress and Laplacian matrices. This approach maintained constraint invariance under additional configurations, providing a robust solution for distributed event-triggered affine formation control in autonomous surface vehicles operating in complex environments [13].

In related studies, Pang et al. extended their approach to non-planar 3D AUV formations, while Chen et al. examined affine formation control for satellite constellations that must navigate obstacles. This research focused on defining leader satellite trajectories to avoid obstacles and establishing an affine formation strategy to ensure follower satellites align with the leader's movements through obstacles [14]. Chen proposed a distributed formation control algorithm to enable follower satellites to reach their target positions [15]. Onuoha et al. proposed a distributed affine formation control method using estimators for multi-agent systems where only the leader is aware of the necessary formation maneuvers, effectively achieving the desired configuration [16]. Xu et al. proposed a distributed finite-time sliding mode estimator, allowing agents to estimate positions, velocities, and accelerations even when only a portion of the leaders and followers have access to formation data. They also devised a two-layer distributed control strategy, incorporating distinct control laws for leaders and an affine control protocol for followers, effectively addressing the affine formation control challenge in Euler–Lagrange systems with output constraints [17].

Expanding on these developments, Chen et al. investigated affine formation control applied to higher-order multi-agent systems, utilizing a two-layer leader–follower structure [18]. In this setup, agents are classified as primary leaders, secondary leaders, and

followers. Primary leaders establish the formation's movement parameters and design general motion strategies, while secondary leaders work together to preserve the desired shape by upholding relative positions. Followers are guided to target positions defined by affine transformations from the leaders, facilitating synchronized movement and formation shape control. This tiered leader–follower structure improves task distribution and coordination, enhancing multi-agent system control. Meanwhile, Onuoha et al. examined distributed adaptive affine formation control for multi-agent systems with linear dynamics and parametric uncertainties, proposing a fully adaptive distributed solution that can handle a range of scenarios, including those with uncertainties in a fully distributed configuration [19]. Luo et al. investigated adaptive affine formation control in systems affected by external disturbances, designing an adaptive control strategy that allows agents to estimate disturbances and then applying an affine formation controller for maneuvers such as translation, scaling, and rotation [20]. Li et al. examined UAV cooperative formation circumnavigation with directed interaction topologies, proposing a distributed affine control method with minimal requirements for global information, forming complex geometric formations with only basic inputs like the formation center, radius, and angular velocity [21].

In recent years, the integration of machine learning into multi-agent systems (MASs) has attracted considerable attention, particularly in addressing control challenges in complex and uncertain environments. Multi-agent reinforcement learning (MARL) has emerged as a promising approach for enabling intelligent decision making and resource allocation. For example, MARL has been employed to optimize resource allocation in UAV networks, achieving efficient coordination under dynamic network conditions [22]. Moreover, surveys such as [23] provide a comprehensive overview of MARL applications, including its use in adaptive control tasks, dynamic collaboration, and distributed decision making in MASs. These studies demonstrate the potential of MARL for enhancing MASs' performance in scenarios involving uncertainty and dynamic changes. In addition to MARL, significant progress has been made in using distributed algorithms and graph-based methods for MASs control. Research has explored robust control strategies to handle environmental uncertainties and improve scalability in multi-robot systems. However, the computational complexity and real-time applicability of machine learning-based approaches remain key challenges, particularly when deployed in resource-constrained systems. Ref. [24] proposes a multi-robot adaptive formation control framework based on deep reinforcement learning, integrating a hybrid control strategy to enable autonomous formation adjustments and collision avoidance in dynamic and complex environments. While learning-based control methods exhibit strong adaptability in handling nonlinear and high-dimensional tasks, they depend on training data and model generalization, which may pose limitations in real-time control and dynamic adaptability for multi-robot systems. In contrast, the proposed method focuses on distributed control strategies, achieving rapid response and formation adjustment without relying on global information. This makes it particularly suitable for practical applications requiring high real-time performance and robustness.

In summary, research on affine formation control has led to notable theoretical advancements and practical implementations, supporting coordinated control and formation adjustments in multi-agent systems. However, maintaining formation stability and ensuring effective task execution in complex, dynamic environments remains a challenging issue due to model uncertainties and environmental disturbances. The Extended State Observer (ESO), as a key technique for disturbance observation and suppression, has gained widespread application and research attention in the field of robotic control in recent years. By estimating unknown disturbances in real time, ESO enables online compensation and the suppression of disturbances, making it an essential component of active disturbance rejection control. Since ESO can simultaneously estimate system states and external disturbances without relying on specific disturbance model information, it demonstrates significant advantages in dealing with complex time-varying disturbances and highly uncertain environments [25]. As ESO continues to be applied in robotic control, researchers are constantly seeking ways to improve its performance. For instance, the

introduction of nonlinear ESO enhances the accuracy of disturbance estimation in complex scenarios and improves noise immunity [26]. Additionally, ESO is often combined with nonlinear control strategies such as sliding mode control to enhance disturbance rejection capabilities, particularly in reducing chattering and improving system stability [27]. However, in practical applications, model parameter uncertainties and disturbances in complex environments can further impact the estimation accuracy and control effectiveness of ESO. As a result, parameter-optimized ESO has become a focus of research. By incorporating parameter optimization techniques, the performance of ESO can be further improved, enabling more accurate disturbance estimation and an adaptive adjustment of observer parameters based on the specific dynamics of the system. This allows ESO to flexibly and precisely handle disturbance estimation and compensation tasks in multidimensional complex disturbances and highly uncertain scenarios. The proposed method in this paper focuses on the problems of formation maintenance and transformation for multi-robot systems in complex obstacle environments. By combining affine formation control with an Extended State Observer (ESO), the method achieves robust control under model parameter uncertainties and environmental disturbances. Compared with existing learning-based control methods, the unique aspects of this study include the following. (1) The integration of stress matrices and affine transformations enables flexible formation adjustments and efficient control for multi-robot systems in complex 2D obstacle environments. (2) The use of ESO allows real-time estimation and compensation for disturbances without relying on extensive training data or offline learning processes, making it more suitable for tasks with high demands on dynamic adaptability and real-time performance.

This paper addresses affine formation tracking control for underactuated robotic formations using an Extended State Observer (ESO) to manage uncertainties in model parameters and external environmental disturbances. It investigates methods for estimating and compensating these disturbances to ensure the system can reliably execute formation transformations—such as translation, rotation, scaling, and shearing—even in challenging conditions. The primary contributions of this work are as follows:

(1) A distributed control strategy is presented, where "leaders define the target formation trajectory, and followers track the formation". By setting clear criteria for leader selection and planning their paths, the formation transformation is guided entirely by the leaders' planned trajectories.
(2) A distributed affine formation control method with disturbance rejection is developed for underactuated robots with "nonlinear, strongly coupled" dynamics, allowing the formation to track target configurations within defined error bounds.
(3) An Extended State Observer (ESO) optimized for parameter estimation is designed to help underactuated robotic formation systems detect and counteract cumulative disturbances arising from model uncertainties and external environmental influences.

2. Preliminaries and Problem Formulation

2.1. Model Description

Consider a group of N robots with the following equations:

$$\begin{cases} \dot{\eta}_i = R(\psi_i)\nu_i \\ \mathscr{M}_i\dot{\nu}_i + \mathscr{C}_i\nu_i + \mathscr{D}_i\nu_i = \mathscr{B}_i\tau_i + \delta_i \end{cases} \tag{1}$$

where $\eta_i = \left[p_i^T, \psi_i\right]^T \in \mathbb{R}^3$ denotes the posture of the ith robot with $p_i = [x_i, y_i]^T$ being its position and ψ_i being its heading angle, $\nu_i = [v_i, \omega_i]^T \in \mathbb{R}^2$ is a vector of linear and angular velocities of the robot, $\mathscr{R}(\psi_i) \in \mathbb{R}^{3\times 2}$ is used to transform the velocity vector ν_i of the robot from its own coordinate system to the global coordinate system. $\tau_i = [\tau_{1,i}, \tau_{2,i}]^T \in \mathbb{R}^2$ is a vector of torque inputs, $\delta_i = [\delta_{1,i}, \delta_{2,i}]^T \in \mathbb{R}^2$ is a vector of time-varying disturbances, $\mathscr{M}_i \in \mathbb{R}^{2\times 2}$ is a symmetric positive-definite inertia matrix, $\mathscr{C}_i \in \mathbb{R}^{2\times 2}$ represents the centripetal and Coriolis forces acting on the ith robot and is bounded, $\mathscr{D}_i \in \mathbb{R}^{2\times 2}$ denotes the damping matrix, and $\mathscr{B}_i \in \mathbb{R}^{2\times 2}$ is the input transformation matrix.

Assumption 1. *Measurements of the robot's posture vector η_i and velocity vector ν_i are available in real time. These measurements are obtained using sensors such as GPS, IMU, encoders, and LiDAR.*

Assumption 2. *The lumped disturbance δ_i and its derivative $\dot{\delta}_i$ are both constrained within known limits. Specifically, (i) δ_i is limited by a specified constant, namely $\| \delta_i \| \leq \varpi_i$, where ϖ_i is a positive constant; (ii) $\dot{\delta}_i$ is also confined within bounds, with $\| \dot{\delta}_i \| \leq \overline{\varpi}_i$, where $\overline{\varpi}_i$ is a positive constant.*

Remark 1. *In real-world scenarios, disturbances such as wind, friction, and payload variations can be estimated and kept within known limits. Modeling these disturbances as bounded allows for the design of robust control algorithms that ensure stability and performance despite the presence of uncertainties. Assumption 2 simplifies the analysis and design of control systems, making it easier to guarantee the desired performance under a variety of operating conditions.*

2.2. Definitions for Affine Transformation

In robot formation control, undirected graphs are widely used to represent communication and interaction relationships among robots. The structure of an undirected graph ensures that each robot has a symmetric relationship with its neighboring robots, aligning well with the mutual perception and cooperation needed for formation tasks. By modeling the formation as an undirected graph $\mathcal{G} = \{\mathcal{V}, \mathcal{E}\}$, where $\mathcal{V}$ represents the robot nodes and $\mathcal{E}$ represents undirected edges, communication links between robots can be effectively described—if there is an edge (A, B) between robots A and B, they can communicate and share information bidirectionally. The characteristics of the undirected graph model make it suitable for achieving formation connectivity, formation maintenance, and formation transformation. By designing specific adjacency relationships and control algorithms in the graph, robot formations can achieve flexible cooperation while ensuring formation stability and task accomplishment. Let $\beth$ represent a nominal configuration associated with the graph $\mathcal{G}$, which can be expressed as $\beth = \left[\beth_l^T, \beth_f^T\right]^T = [\lambda_1, \lambda_2, \cdots, \lambda_N]^T$. Below, we introduce some essential definitions and lemmas related to affine transformation.

Definitions 1 ([10])**.** *Consider the formation $(\mathcal{G}, \beth)$, where $\ell_{ij} \in \mathbb{R}$ represents a stress associated with edge $(i, j) \in \mathcal{E}$. This stress is a scalar quantity satisfying $\ell_{ij} = \ell_{ji}$. Let $\mathfrak{F}$ denote the set comprising all ℓ_{ij} , which is treated as an equilibrium stress set if, for each $i \in \mathcal{V}$ and $j \in \mathcal{N}_i$ (where $\mathcal{N}_i$ denotes the neighbors of node i in the graph), the following equality is met:*

$$(\mathfrak{F} \otimes I_2)\beth = 0 \tag{2}$$

where $\mathfrak{F} \in \mathbb{R}^{2\times 2}$ satisfies:

$$[\mathfrak{F}]_{ij} = \begin{cases} 0 & i \neq j, (i,j) \notin \mathcal{E} \\ -\ell_{ij} & i \neq j, (i,j) \in \mathcal{E} \\ \sum\limits_{k \in \mathcal{N}_i} \ell_{ik} & i = j \end{cases} \tag{3}$$

Definitions 2 ([10])**.** *In the context of the formation $(\mathcal{G}, \beth)$, the affine span of the nominal configuration $\{\lambda_i\}_{i=1}^N$ can be described as follows:*

$$A = \left\{ \sum_{i=1}^{N} \alpha_i \lambda_i | \lambda_i \in \mathbb{R}^2, \alpha_i \in \mathbb{R} \text{ and } \sum_{i=1}^{N} \alpha_i = 1 \right\} \tag{4}$$

Definitions 3 ([10]). *The affine image refers to the set that includes all affine transformations of the nominal configuration* $\{\lambda_i\}_{i=1}^N$ *and is defined as follows:*

$$S(\beth) = \left\{ P = \left[p_1^T, p_2^T, \cdots, p_N^T \right]^T \in \mathbb{R}^{2N} \middle| p_i = A\lambda_i + \mathscr{b} \right\} \tag{5}$$

where $A \in \mathbb{R}^{2\times 2}$ *and* $\mathscr{b} \in \mathbb{R}^2$ *are the parameters of the affine transformation. The schematic diagram of the affine transformation is shown in Figure 1.*

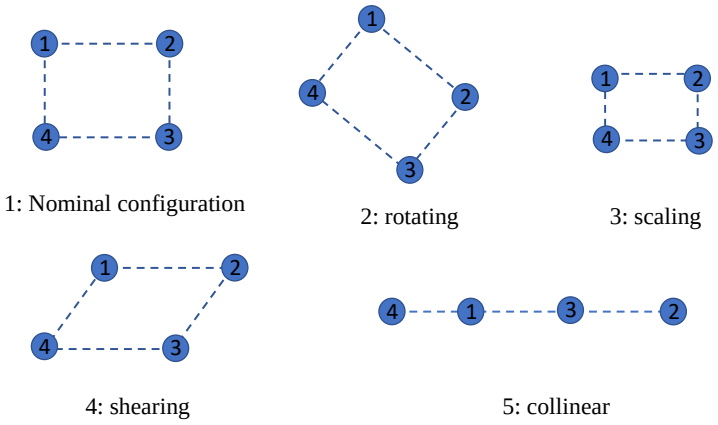


Figure 1. Affine formation maneuver.

Definitions 4 ([10]). *The formation* $(\mathscr{G}, \beth)$ *is considered affinely localizable if the following two conditions are met: (i) the set* $\{\lambda_i\}_{i=1}^N$ *must affinely span* $\mathbb{R}^2$*; (ii) for any* $P = \left[P_l^T, P_f^T \right]^T \in A(\beth)$*, the component* P_f *can be uniquely determined by* P_l*.*

Lemma 1 ([10]). *An augmented matrix* $\overline{\beth} = [\beth, \mathbf{1}_N] \in \mathbb{R}^{N\times 3}$ *ensures that the nominal configuration* $\{\lambda_i\}_{i=1}^N$ *affinely spans* $\mathbb{R}^2$ *if and only if* $N \geq 3$ *and* $rank\left(\overline{\beth}\right) = 3$*.*

Lemma 2 ([10]). *The nominal configuration* $(\mathscr{G}, \beth)$ *is considered universally rigid if and only if there exists a stress matrix* $\mathfrak{F}$ *that is positive semi-definite and has a rank of* $N - 3$*.*

Lemma 3 ([10]). *Under the condition that* $\{\lambda_i\}_{i=1}^N$ *affinely spans* $\mathbb{R}^2$*, the nominal configuration* $(\mathscr{G}, \beth)$ *is affinely localizable if and only if the subset* $\{\lambda_i\}_{i\in N_l}$ *also affinely spans* $\mathbb{R}^2$*.*

Lemma 4 ([10]). *For the stress matrix, let*

$$\overline{\beth} = \beth \otimes I_2 = \begin{bmatrix} \overline{\beth}_{ll} & \overline{\beth}_{lf} \\ \overline{\beth}_{fl} & \overline{\beth}_{ff} \end{bmatrix} \tag{6}$$

where $\overline{\beth}_{fl} \in \mathbb{R}^{2N_f\times 2N_l}$ *and* $\overline{\beth}_{ff} \in \mathbb{R}^{2N_f\times 2N_f}$*. If the nominal configuration* $\{\lambda_i\}_{i=1}^N$ *affinely spans* $\mathbb{R}^2$ *and has a positive semi-definite stress matrix* $\beth$*, then it is affinely localizable if and only if* $\overline{\beth}_{ff}$ *is invertible. When* $\overline{\beth}_{ff}$ *is invertible, for any* $\left[p_l^T, p_f^T \right]^T \in A(\beth)$*,* p_f *can be uniquely determined by* $p_f = -\overline{\beth}_{ff}^{-1}\overline{\beth}_{fl}p_l$*.*

2.3. Control Objective

The control objective is to achieve arbitrary formation transformations and accomplish formation tasks for a group of robots even in the presence of obstacles, model parameter uncertainties, and environmental disturbances. The formation control system should ensure that the robots can dynamically adjust their positions and orientations to maintain the

desired formation pattern, avoid collisions with obstacles, and compensate for uncertainties and disturbances. This includes real-time obstacle detection and avoidance, adaptive control strategies to handle parameter variations, and robust control methods to mitigate the impact of external disturbances, thereby enabling the successful execution of formation tasks under varying and challenging conditions, i.e.,

$$\begin{aligned} &\lim_{t\to\infty}\left(p_l(t)-\mathcal{p}_l^*(t)\right)=0\\ &\lim_{t\to\infty}\left(p_f(t)+\overline{\mathcal{D}}_{ff}^{-1}\overline{\mathcal{D}}_{fl}\mathcal{p}_l\right)=0. \end{aligned} \tag{7}$$

3. Affine Formation Maneuver Control Design

The control design procedure is organized into two key steps:

Step 1: In this part, a leader–follower strategy is applied, where the overall formation's affine transformation is achieved by controlling the positions of the leaders. It is assumed that only a select group of robots, designated as leaders, are aware of the intended formation maneuver. According to Lemma 4, these leaders uniquely determine the followers' paths. For the leaders' trajectory planning, reference can be made to [1].

The desired formation trajectory is defined as $\mathcal{p}^* = \left[\mathcal{p}_l^*, \overline{\mathcal{D}}_{ff}^{-1}\overline{\mathcal{D}}_{fl}\mathcal{p}_l\right]^T = \left[\mathcal{p}_1^*, \mathcal{p}_2^*, \cdots, \mathcal{p}_N^*\right]^T$. Initially, we define the relevant variables for the ith robot:

$$\begin{cases} \mathcal{X}_i \triangleq \dot{\mathcal{p}}_{1,i}^* - k_1 \tanh\frac{\widetilde{x}_i}{k_1} \\ \mathcal{Y}_i \triangleq \dot{\mathcal{p}}_{2,i}^* - k_2 \tanh\frac{\widetilde{y}_i}{k_2} \\ \widetilde{x}_i \triangleq x_i - \mathcal{p}_{1,i}^* \\ \widetilde{y}_i \triangleq y_i - \mathcal{p}_{2,i}^* \end{cases} \tag{8}$$

where $\mathcal{p}_{1,i}^*$ and $\mathcal{p}_{2,i}^*$ are the first and second elements of $\mathcal{p}_i^*$ ($i = 1, 2, \cdots, N$), $\dot{\mathcal{p}}_{1,i}^*$ and $\dot{\mathcal{p}}_{2,i}^*$ are the derivatives of $\mathcal{p}_{1,i}^*$ and $\mathcal{p}_{2,i}^*$; k_1 and k_2 are a positive constant.
Reorganizing Equation (8) with the ith robot's kinematic equations, we obtain

$$\begin{cases} \dot{\widetilde{x}}_i + k_{1,i}\tanh\frac{\widetilde{x}_i}{k_{1,i}} = v_i\cos\psi_i - \mathcal{X}_i \\ \dot{\widetilde{y}}_i + k_{2,i}\tanh\frac{\widetilde{y}_i}{k_{2,i}} = v_i\sin\psi_i - \mathcal{Y}_i \end{cases} \tag{9}$$

According to the control objectives in Section 2.3, it is known that the tracking error needs to approach zero. Therefore, combining Equation (9), we understand that to achieve the control objectives, the right-hand side of Equation (9) needs to approach zero. Then, one has

$$\begin{cases} \cos\psi_i e_{1,i} + \sin\psi_i e_{2,i} = v_i - \cos\psi_i\mathcal{X}_i - \sin\psi_i\mathcal{Y}_i \\ -\sin\psi_i e_{1,i} + \cos\psi_i e_{2,i} = \sin\psi_i\mathcal{X}_i - \cos\psi_i\mathcal{Y}_i \end{cases} \tag{10}$$

where $e_{1,i} = v_i\cos\psi_i - \mathcal{X}_i$ and $e_{2,i} = v_i\sin\psi_i - \mathcal{Y}_i$.

The virtual heading angle, which is determined by the tangent angle of the variables $\mathcal{X}_i$ and $\mathcal{Y}_i$, is also proposed to guide the follower toward its desired state:

$$\psi_i^* = \operatorname{atan2}\frac{\mathcal{Y}_i}{\mathcal{X}_i} \tag{11}$$

Therefore, the design of the virtual velocity control law is as follows

$$\begin{cases} v_i^* = \cos\left(\psi_i - \psi_i^*\right)\sqrt{\left(\mathcal{X}_i\right)^2 + \left(\mathcal{Y}_i\right)^2} \\ \omega_i^* = -k_{3,i}\tanh\frac{\widetilde{\psi}_i}{k_{3,i}} + \dot{\psi}_i^* \end{cases} \tag{12}$$

where $\widetilde{\psi}_i = \psi_i - \psi_i^* k_3$, is a positive constant.

Introduce the following auxiliary error variables

$$\begin{cases} \varkappa_{1,i} = v_i - v_i^* \\ \varkappa_{2,i} = \omega_i - \omega_i^* \end{cases} \tag{13}$$

The torque control input for the ith robot can be chosen as follows

$$\tau_i = \mathscr{B}_i^{-1}\left(-\begin{bmatrix} k_{4,i} & 0 \\ 0 & k_{5,i} \end{bmatrix}\begin{bmatrix} \varkappa_{1,i} \\ \varkappa_{2,i} \end{bmatrix} + \mathscr{M}_i\dot{\nu}_i + \mathscr{C}_i\nu_i + \mathscr{D}_i\nu_i - \delta_i\right) \tag{14}$$

where $k_{4,i}$ and $k_{5,i}$ are positive constants.

Step 2: In the control of robotic systems, the influence of different types of disturbances and uncertainties on system performance is significant. To improve system robustness and accuracy, it is essential to effectively model and compensate for these disturbances. For simplified analysis and control design, we group these various disturbance terms into a lumped disturbance $\mathscr{W}_i = [\mathscr{W}_{1,i}, \mathscr{W}_{2,i}]^T$, which is defined as follows:

$$\mathscr{W}_i = \delta_i - \mathscr{C}_i\nu_i - \mathscr{D}_i\nu_i \tag{15}$$

The definition of the lumped disturbance $\mathscr{W}_i$ effectively integrates the various disturbances and uncertainties present in the system. This unified approach facilitates the handling and compensation of these disturbances, thereby simplifying the controller design and enhancing the robustness of the system.

Let $\varphi_i = [v_i, \omega_i, \mathscr{W}_{1,i}, \mathscr{W}_{2,i}]^T$ and $u_i = \mathscr{M}_i^{-1}[\tau_{1,i}, \tau_{2,i}]^T$, and rewriting (1) in state-space form, one has

$$\dot{\varphi}_i = \mathscr{g}_i\varphi_i + u_i + \mathscr{q}_i\ell_i \tag{16}$$

where $\mathscr{g}_i = \begin{bmatrix} 0_{2\times2} & I_{2\times2} \\ 0_{2\times2} & 0_{2\times2} \end{bmatrix}$, $\mathscr{q}_i = \begin{bmatrix} 0_{2\times2} \\ I_{2\times2} \end{bmatrix}$, $\ell_i = \begin{bmatrix} \dot{\mathscr{W}}_{1,i}, \dot{\mathscr{W}}_{2,i} \end{bmatrix}^T$. The observer is proposed:

$$\dot{\hat{\varphi}}_i = \mathscr{g}_i\hat{\varphi}_i + u_i + \hbar_i\mathscr{s}_i\widetilde{\varphi}_i \tag{17}$$

where $\hat{\varphi}_i = \begin{bmatrix} \hat{v}_i, \hat{\omega}_i, \hat{\mathscr{W}}_{1,i}, \hat{\mathscr{W}}_{2,i} \end{bmatrix}^T$ is the estimation of φ_i, $\widetilde{\varphi}_i = \varphi_i - \hat{\varphi}_i$ is the estimation error, and $\mathscr{s}_i = \begin{bmatrix} I_{2\times2} & 0_{2\times2} \end{bmatrix}$, $\hbar_i \in \mathbb{R}^{4\times2}$ represent the constant observer gain, which is suggested to be determined as follows:

$$\hbar_i = -\xi_i^T\mu_i \tag{18}$$

where $\xi_i \in \mathbb{R}^{4\times4}$ and $\mu_i \in \mathbb{R}^{4\times2}$ are components of the optimization problem's solution, which are obtainable through certain Linear Matrix Inequalities (LMIs)

$$\begin{aligned} &\min_{\xi_i,\mu_i,\sigma_i} \sigma_i \\ &s.t.\ \xi_i > 0, \\ &\quad \mathscr{g}_i^T\xi_i + \xi_i\mathscr{g}_i + \mathscr{s}_i^T\mu_i^T + \mu_i\mathscr{s}_i + I \le 0 \\ &\quad \begin{bmatrix} -\sigma_i I & \xi_i\mathscr{q}_i \\ * & -\sigma_i \end{bmatrix} \le 0 \end{aligned} \tag{19}$$

where $\sigma_i \in \mathbb{R}$ serves as the decision variable. The suggested affine formation tracking control method, which includes disturbance estimation, is outlined as follows:

$$\tau_i = \mathscr{B}_i^{-1}\left(-\begin{bmatrix} k_4 & 0 \\ 0 & k_5 \end{bmatrix}\begin{bmatrix} e_{1i} \\ e_{2i} \end{bmatrix} + \mathscr{M}_i\dot{\nu}_i - \hat{\mathscr{W}}_i\right) \tag{20}$$

Equation (16) establishes the state-space model of the system. Equation (17) designs the Extended State Observer (ESO) for disturbance estimation. Equations (18) and (19) apply the LMI optimization method to ensure the performance of the observer and the

control system. Finally, Equation (20) develops the affine formation control strategy to achieve robust tracking of the target formation.

4. Stability Analysis

Theorem 1. *Given Assumptions 1 and 2, consider the formation system described in Equation (1). By applying the anti-disturbance affine formation maneuver control strategy, which combines the disturbance observer (17) with the formation tracking controller, all signals within the closed-loop system remain bounded.*

Proof. The candidate Lyapunov function is selected as

$$V_i = V_{1,i} + V_{2,i} + V_{3,i} \tag{21}$$

The candidate Lyapunov functions $V_{1,i}$, $V_{2,i}$ and $V_{3,i}$ are selected as

$$V_{1,i} = \frac{1}{2}\widetilde{\varphi}_i^T P_i \widetilde{\varphi}_i \tag{22}$$

$$V_{2,i} = k_1 \ln\left(\cosh\frac{\widetilde{x}_i}{k_1}\right) + k_2 \ln\left(\cosh\frac{\widetilde{y}_i}{k_2}\right) + k_3 \ln\left(\cosh\frac{\widetilde{\psi}_i}{k_3}\right) \tag{23}$$

$$V_{3,i} = \frac{1}{2}\varkappa_{1,i}^2 + \frac{1}{2}\varkappa_{2,i}^2 \tag{24}$$

Taking the derivative of $\widetilde{\varphi}_i$, one has

$$\dot{\widetilde{\varphi}}_i = (\mathcal{G}_i - \hbar_i \jmath_i)\widetilde{\varphi}_i + \mathcal{G}_i h_i \tag{25}$$

By integrating the above equations, the derivative of Equation (22) is obtained as follows:

$$\dot{V}_{1,i} = \frac{1}{2}\widetilde{\varphi}_i^T \left((\mathcal{G}_i - \hbar_i \jmath_i)^T \xi_i + \xi_i (\mathcal{G}_i - \hbar_i \jmath_i) \right) \widetilde{\varphi}_i + \widetilde{\varphi}_i^T \xi_i \mathcal{G}_i \ell_i \tag{26}$$

Let $\mu_i = -\xi_i \hbar_i$, rewrite (26) as

$$\dot{V}_{1,i} = \frac{1}{2}\widetilde{\varphi}_i^T \left(\mathcal{G}_i^T \xi_i + \xi_i \mathcal{G}_i + \hbar_i^T \mu_i^T + \mu_i \hbar_i \right) \widetilde{\varphi}_i + \widetilde{\varphi}_i^T \xi_i \mathcal{G}_i \ell_i \tag{27}$$

If the third inequality in Equation (19) holds, then we have

$$\begin{aligned} \dot{V}_{1,i} &\leq -\frac{1}{2} \parallel \widetilde{\varphi}_i \parallel^2 + \parallel \widetilde{\varphi}_i \parallel \parallel \xi_i \mathcal{G}_i \parallel \parallel \ell_i \parallel \\ &\leq -\frac{1}{2}(1-\theta_i) \parallel \widetilde{\varphi}_i \parallel^2 \end{aligned} \tag{28}$$

where $0 < \theta_i < 1$, and $\parallel \widetilde{\varphi}_i \parallel \geq \frac{2\|\xi_i \mathcal{G}_i\| \|\ell_i\|}{\theta_i}$. According to Assumption 1, one has

$$\parallel \widetilde{\varphi}_i \parallel (t) \leq \max\{\Xi(\parallel \widetilde{\varphi}_i(0) \parallel, t), \aleph(\parallel \ell_i \parallel)\} \tag{29}$$

where $\Xi(\cdot)$ is the $\mathscr{KL}$ function, and $\aleph(\cdot)$ is the $\mathscr{K}_\infty$ function defined as

$$\aleph(\parallel \ell_i \parallel) = \sqrt{\frac{\lambda_{\max}(\xi_i)}{\lambda_{\min}(\xi_i)}} \frac{2 \parallel \xi_i \mathcal{G}_i \parallel \parallel \ell_i \parallel}{\theta_i} \tag{30}$$

Therefore, the estimation dynamics exhibit ISS properties with respect to ℓ_i.

Recalculating the first and second equations in (1), one has

$$\begin{aligned}\dot{x}_i &= e_{1,i}\cos\psi_i + v_i^*\cos\psi_i \\ &= e_{1,i}\cos\psi_i + \cos^2\psi_i\mathcal{X}_i + \sin\psi_i\cos\psi_i\mathcal{Y}_i \\ &= e_{1,i}\cos\psi_i + \cos^2\psi_i\mathcal{X}_i \\ &\quad + \sin\psi_i(\cos\psi_i^*\mathcal{Y}_i + (\cos\psi_i - \cos\psi_i^*)\mathcal{Y}_i) \\ &= e_{1,i}\cos\psi_i + \mathcal{X}_i \\ &\quad + \sin\psi_i((\sin\psi_i^* - \sin\psi_i)\mathcal{X}_i + (\cos\psi_i - \cos\psi_i^*)\mathcal{Y}_i) \\ &= e_{1,i}\cos\psi_i + \mathcal{X}_i + \Gamma_i\sin\psi_i\end{aligned} \tag{31}$$

$$\begin{aligned}\dot{y}_i &= e_{1,i}\sin\psi_i + v_i^*\sin\psi_i \\ &= e_{1,i}\sin\psi_i + \sin^2\psi_i\mathcal{Y}_i + \cos\psi_i\sin\psi_i\mathcal{X}_i \\ &= e_{1,i}\sin\psi_i + \sin^2\psi_i\mathcal{Y}_i \\ &\quad + \cos\psi_i(\sin\psi_i^*\mathcal{X}_i + (\sin\psi_i - \sin\psi_i^*)\mathcal{X}_i) \\ &= e_{1,i}\sin\psi_i + \mathcal{Y}_i \\ &\quad + \cos\psi_i((\cos\psi_i^* - \cos\psi_i)\mathcal{Y}_i + (\sin\psi_i - \sin\psi_i^*)\mathcal{X}_i) \\ &= e_{1,i}\sin\psi_i + \mathcal{Y}_i - \Gamma_i\cos\psi_i\end{aligned} \tag{32}$$

where Γ_i satisfies

$$\begin{aligned}\Gamma_i &= -(\sin\psi_i - \sin\psi_i^*)\mathcal{X}_i + (\cos\psi_i - \cos\psi_i^*)\mathcal{Y}_i \\ &= -2\sin\frac{\widetilde{\psi}_i}{2}\left(\cos\frac{\psi_i + \psi_i^*}{2}\mathcal{X}_i + \sin\frac{\psi_i + \psi_i^*}{2}\mathcal{Y}_i\right)\end{aligned} \tag{33}$$

It is important to point out that Γ_i is bounded because $\mathcal{X}_i$ and $\mathcal{Y}_i$ are bounded, and hence, it approaches zero as $\widetilde{\psi}_i$ approaches zero.

Then, the derivatives of the position and orientation tracking errors of the ith robot can be derived as follows:

$$\dot{\widetilde{x}}_i = -k_1\tanh\frac{\widetilde{x}_i}{k_1} + e_{1,i}\cos\psi_i + \Gamma_i\sin\psi_i \tag{34}$$

$$\dot{\widetilde{y}}_i = -k_2\tanh\frac{\widetilde{y}_i}{k_2} + e_{1,i}\sin\psi_i - \Gamma_i\cos\psi_i \tag{35}$$

$$\dot{\widetilde{\psi}}_i = -k_3\tanh\frac{\widetilde{\psi}_i}{k_3} \tag{36}$$

Let $\zeta_{1,i} = \tanh\frac{\widetilde{x}_i}{k_1}$, $\zeta_{2,i} = \tanh\frac{\widetilde{y}_i}{k_2}$, and $\zeta_{3,i} = \tanh\frac{\widetilde{\psi}_i}{k_3}$. Taking the derivative of $V_{2,i}$ and $V_{3,i}$, one has

$$\begin{aligned}\overline{V}_i &= \dot{V}_{2,i} + \dot{V}_{3,i} \\ &= -k_1\zeta_{1,i}^2 - k_2\zeta_{2,i}^2 - k_3\zeta_{3,i}^2 - k_4\varkappa_{1,i}^2 - k_5\varkappa_{2,i}^2 + k_1e_{1,i}\cos\psi_i \\ &\quad + k_2\Gamma_i\sin\psi_i + k_2e_{1,i}\sin\psi_i - k_2\Gamma_i\cos\psi_i \\ &\quad + \varkappa_{1,i}\widetilde{\varphi}_{3,i} + \varkappa_{2,i}\widetilde{\varphi}_{4,i}\end{aligned} \tag{37}$$

where $\widetilde{\varphi}_{3,i}$ and $\widetilde{\varphi}_{4,i}$ are the third and fourth elements of $\widetilde{\varphi}_i$. Based on the fact that the estimation dynamics are ISS with respect to ℓ_i, it can be concluded that the disturbance estimation errors of the robot are bounded. Additionally, there exists a constant such that $|\widetilde{\varphi}_{3,i}| \le \iota_{3,i}$ and $|\widetilde{\varphi}_{4,i}| \le \iota_{4,i}$. By applying Young's inequality and reorganizing (37), one has

$$\overline{V}_i \le -\overline{k}_1\zeta_{1,i}^2 - \overline{k}_2\zeta_{2,i}^2 - \overline{k}_3\zeta_{3,i}^2 - \overline{k}_4\varkappa_{1,i}^2 - \overline{k}_5\varkappa_{2,i}^2 + \varpi_i \tag{38}$$

where $\bar{k}_1 > \frac{3}{4}, \bar{k}_2 > \frac{3}{4}, \bar{k}_3 > \frac{1}{2}, \bar{k}_4 > \frac{5}{4}, \bar{k}_5 > \frac{3}{4}$; $\varpi_i = 2\Gamma_i^2 + \iota_{3,i}^2 + \iota_{4,i}^2$. According to (37) and (38), the position tracking error of the ith robot, $\zeta_{1,i}$, $\zeta_{2,i}$, $\zeta_{3,i}$, $\varkappa_{1,i}$ and $\varkappa_{2,i}$ are ultimately bounded. □

5. Simulation

The robot formation simulation is implemented in MATLAB R2021b with a simulation duration of 330 s and a control period of 1 ms. The overall robot formation control framework adopts a leader–follower structure. The specific parameters of the robots refer to [28]. According to Lemma 2, three robots are selected as virtual leaders in the simulation, while the remaining four robots are designated as followers. The followers are numbered as "Robot 1", "Robot 2", "Robot 3", and "Robot 4", respectively. Taking the point (0,0) as the reference point, the formation layout of all the leaders and followers is as follows: (20,0), (10,10), (10,−10), (0,10), (0,−10), (−10,10), and (−10,−10). The communication topology of the formation system is shown in Figure 2.

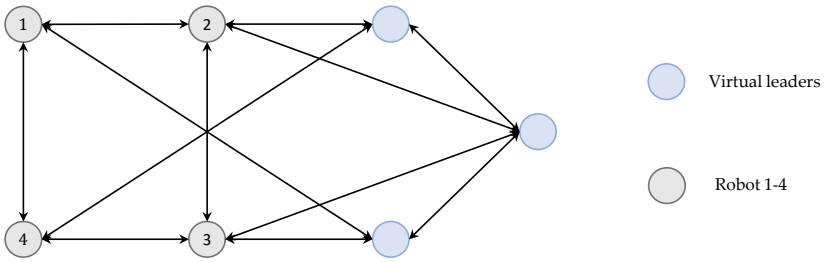


Figure 2. Communication topology.

By incorporating the communication topology between formations and drawing on the methodology outlined in [10], the stress matrix for the formations can be determined. The resulting stress matrix in this study is presented as follows:

$$\overline{\beth} = \begin{bmatrix} -0.2741 & 0.2741 & 0.2741 & -0.1370 & -0.1370 & 0 & 0 \\ 0.2741 & -0.6852 & 0 & 0.5482 & 0 & 0 & -0.1370 \\ 0.2741 & 0 & -0.6852 & 0 & 0.5482 & -0.1370 & 0 \\ -0.1370 & 0.5482 & 0 & -0.7537 & 0.0685 & 0.2741 & 0 \\ -0.1370 & 0 & 0.5482 & 0.0685 & -0.7537 & 0 & 0.2741 \\ 0 & 0 & -0.1370 & 0.2741 & 0 & -0.2741 & 0.1370 \\ 0 & -0.1370 & 0 & 0 & 0.2741 & 0.1370 & -0.1370 \end{bmatrix} \tag{39}$$

The initial position vectors for the three leaders are set as $\eta_1 = [450, 410, 0]^T$, $\eta_2 = [380, 370, 0]^T$, and $\eta_3 = [320, 320, 0]^T$ with velocities $\nu_1 = [0, 0]^T$, $\nu_2 = [0, 0]^T$ and $\nu_3 = [0, 0]^T$. Similarly, the four followers have initial position vectors $\eta_4 = [450, 430, 0]^T$, $\eta_5 = [460, 420, 0]^T$, $\eta_6 = [465, 440, 0]^T$, and $\eta_7 = [480, 420, 0]^T$ and velocity vectors $\nu_4 = [0, 0]^T$, $\nu_5 = [0, 0]^T$, $\nu_6 = [0, 0]^T$, and $\nu_7 = [0, 0]^T$. The unknown external random disturbance applied to the wheel speed systems of the leaders and followers is chosen as $\delta_i = [10\sin(0.02t) + 2\cos(0.6t), 10\sin(0.6t) + 2\cos(0.02t)]^T$.

The controller parameters are set as $k_{1,i} = 2$, $k_{2,i} = 4$, $k_{3,i} = 1.5$, $k_{4,i} = 1$, $k_{5,i} = 1$, and $i = 1, 2, \cdots, 7$. By employing YALMIP to solve (18) and (19), we have

$$\xi_i = \begin{bmatrix} 5.2780 & 0 & -1.5951 & 0 \\ 0 & 5.2780 & 0 & -1.5951 \\ -1.5951 & 0 & 2.6363 & 0 \\ 0 & -1.5951 & 0 & 2.6363 \end{bmatrix} \tag{40}$$

$$\mu_i = \begin{bmatrix} -2.6547 & 0 \\ 0 & -2.6547 \\ -5.2780 & 0 \\ 0 & -5.2780 \end{bmatrix} \tag{41}$$

In this section, to evaluate the estimation performance of the observer optimized through LMI, we compare the gains derived from LMI solutions with those determined based on Lyapunov stability criteria. For cases without LMI optimization, the observer gains are set as $\hbar_1 = \hbar_2 = \hbar_3 = [diag(4,5), diag(5,3)]^T$,$\hbar_4 = \hbar_5 = \hbar_6 = \hbar_7 = [diag(5,2), diag(1,2)]^T$.

In this study, all obstacles are static, such as channel boundaries in the environment. The simulation outcomes are shown in Figures 3–12. In Figure 3, the formation system's motion path is depicted, where the navigation between two gray obstacles replicates the narrow passage environment commonly encountered in robotic survey tasks. Figures 4 and 5 present the tracking errors of the follower agents. Figures 6 and 7 illustrate the Extended State Observer's estimation of the combined disturbances, accounting for environmental interference and model parameter uncertainties, affecting the followers. Figures 10 and 11 depict the forces and torques applied to the followers using the proposed disturbance-rejection affine formation control strategy in this study.

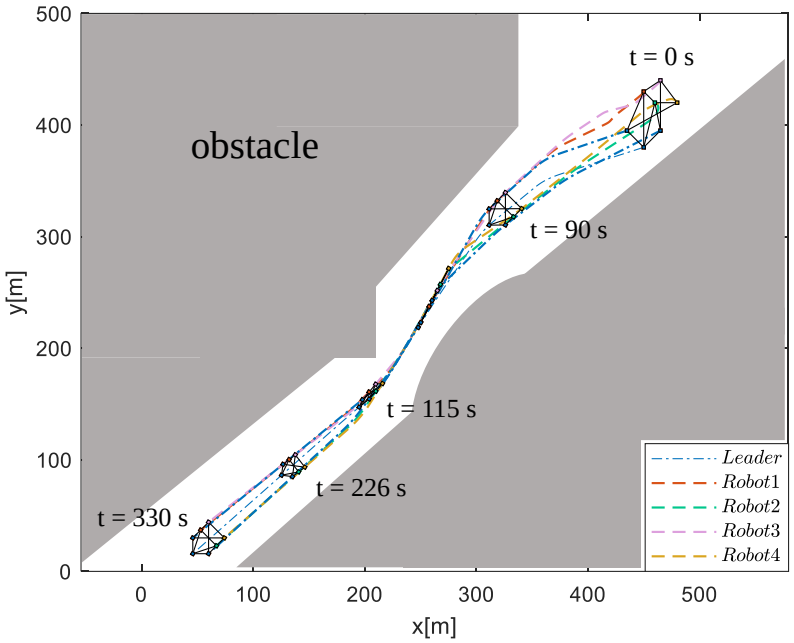


Figure 3. Formation motion trajectories.

According to Theorem 1, with the application of the Extended State Observer (17), velocity control laws (12), and affine formation controllers (20), the intended formation maneuver is successfully achieved. Figure 3 illustrates how the formation system promptly attains the target configuration with the proposed control approach. As the formation nears the channel, its size gradually contracts to ensure safe entry into the narrow passage, preventing any collisions with surrounding static obstacles. Upon entering the channel, the formation rapidly adjusts into a single-line arrangement to enable smooth transit. After passing through the confined area, the formation expands once more to adapt effectively to the wider survey environment. In the simulation setup, significant initial position deviations were intentionally designed to evaluate the performance of the proposed control method under complex conditions. Some robots were placed at considerable distances from their target formation positions, requiring substantial adjustments to converge to the desired trajectories. As a result, the tracking error (Figures 4 and 5) curves exhibited large fluctuations during the initial adjustment phase. However, under the influence of the Extended State Observer (ESO) and affine formation control strategy, the system quickly

suppressed these errors and converged to acceptable levels, demonstrating the robustness and effectiveness of the proposed method in handling complex initial conditions.

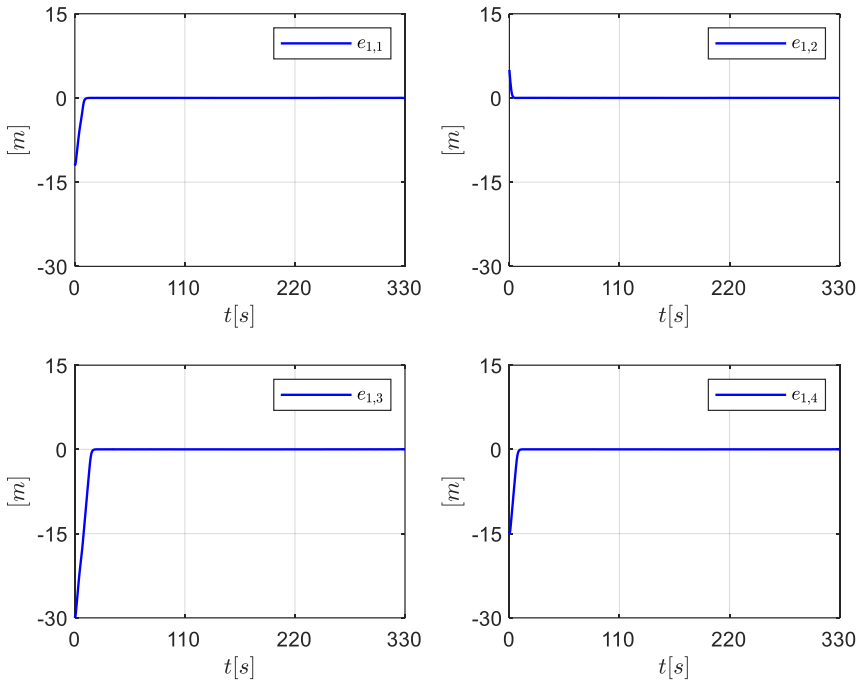


Figure 4. The tracking errors of the followers in x-axis.

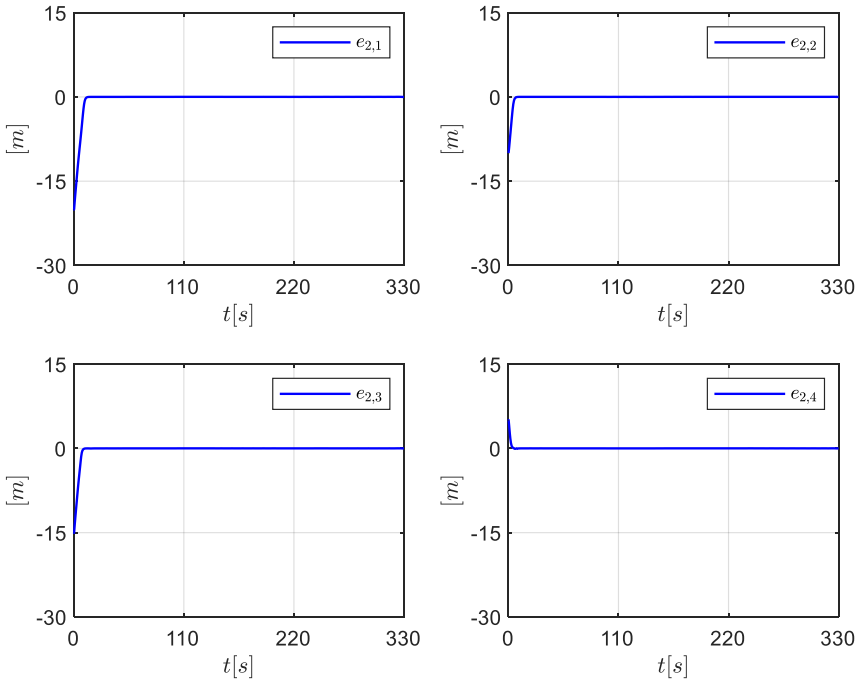


Figure 5. The tracking errors of the followers in y-axis.

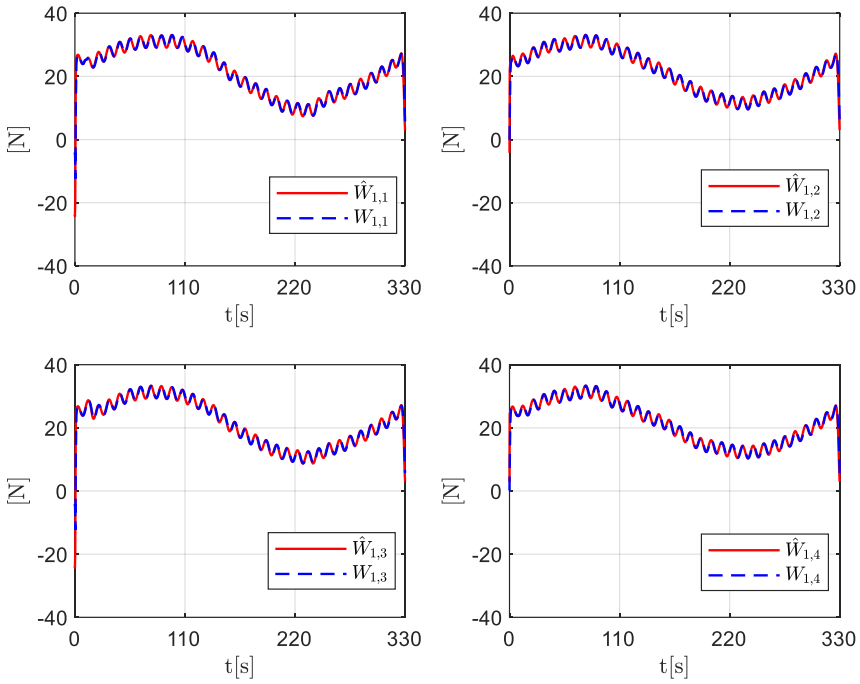


Figure 6. The lumped disturbance estimation of the followers.

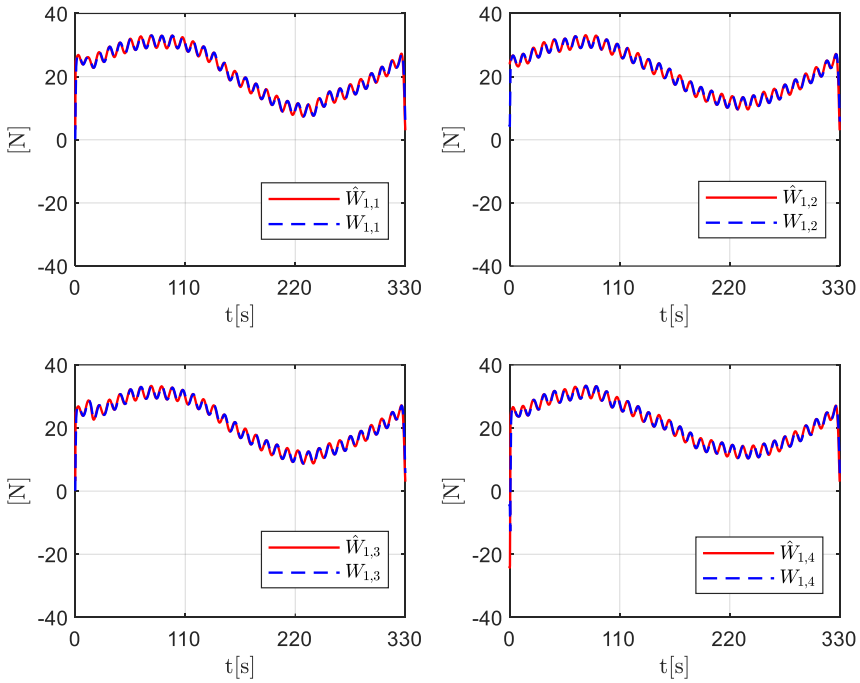


Figure 7. The lumped disturbance estimation of the follower.

Figures 8 and 9 illustrate the observation error when observer gains are determined using the LMI method compared to directly setting the gains. The figures indicate that gains obtained through LMI result in more accurate disturbance estimation than those based on Lyapunov stability conditions. This highlights that the optimization criterion in Equation (19) improves the observer's accuracy and leads to better state estimation. The simulation results validate the effectiveness of the control strategy in achieving the targeted formation maneuvers.

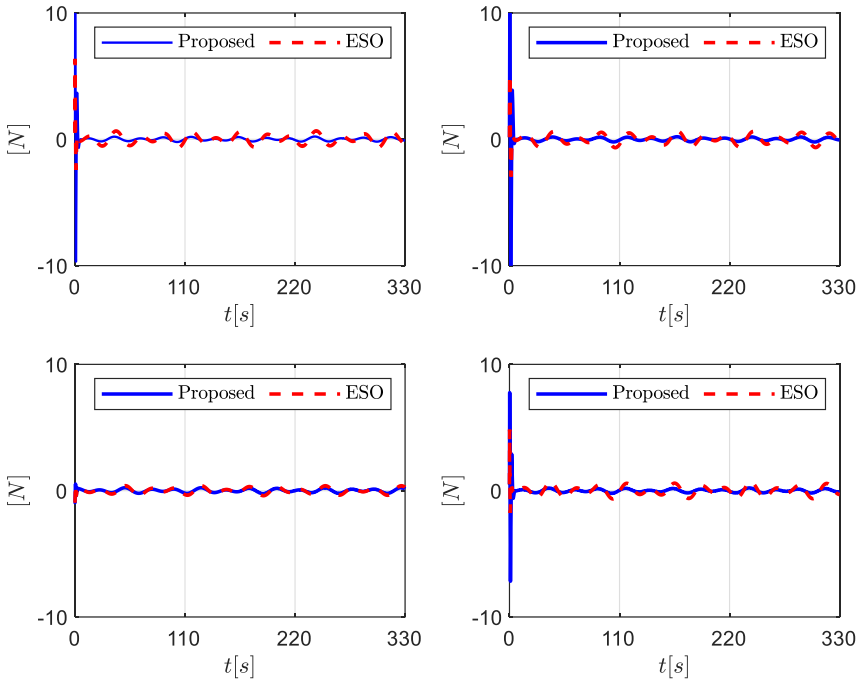


Figure 8. The estimation errors of the followers.

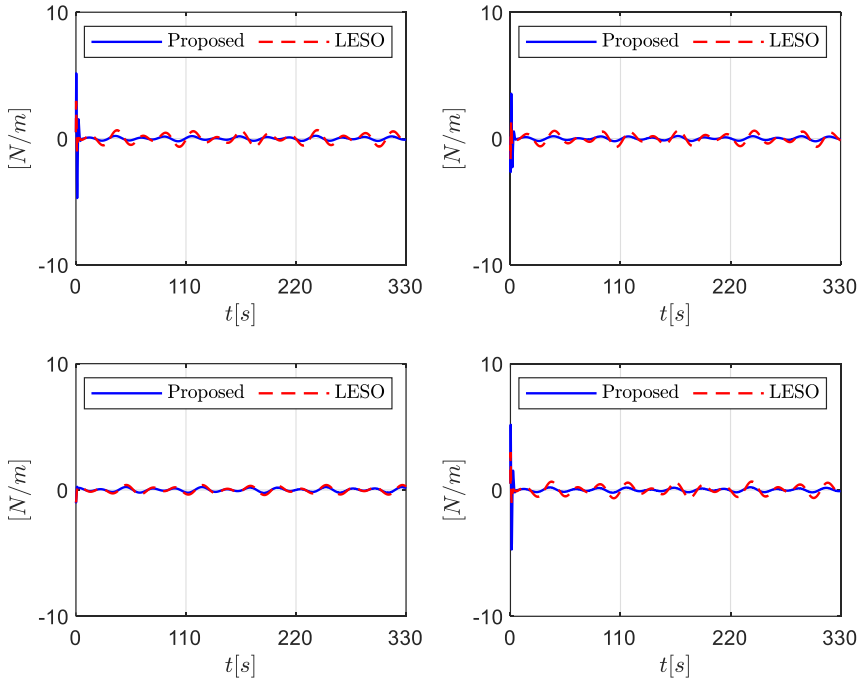


Figure 9. The estimation errors of the followers.

To validate the effectiveness of the affine formation control method proposed in this paper, a comparison is made with the distance-based time-varying control method presented in [4]. Figure 12 shows the formation trajectory under the control method proposed in [4]. Comparing it with Figure 3, it is evident that the method in [4] can only achieve formations with a fixed size and cannot facilitate the collinearity or rotation of the formation. This indicates that the method in [4] has limitations in flexibility and versatility, whereas the affine formation control method proposed in this paper offers enhanced dynamic adjustment capabilities.

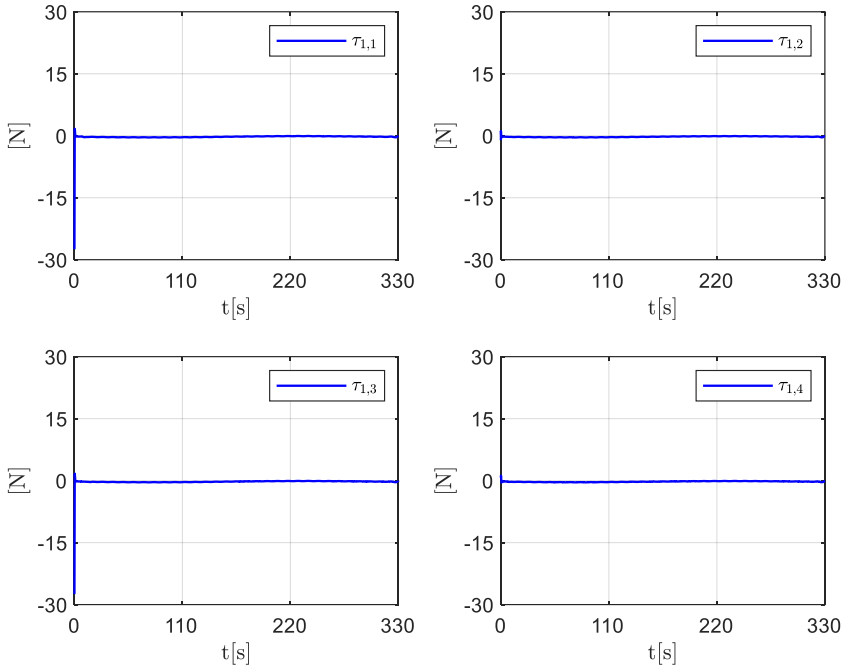


Figure 10. The forces of the followers.

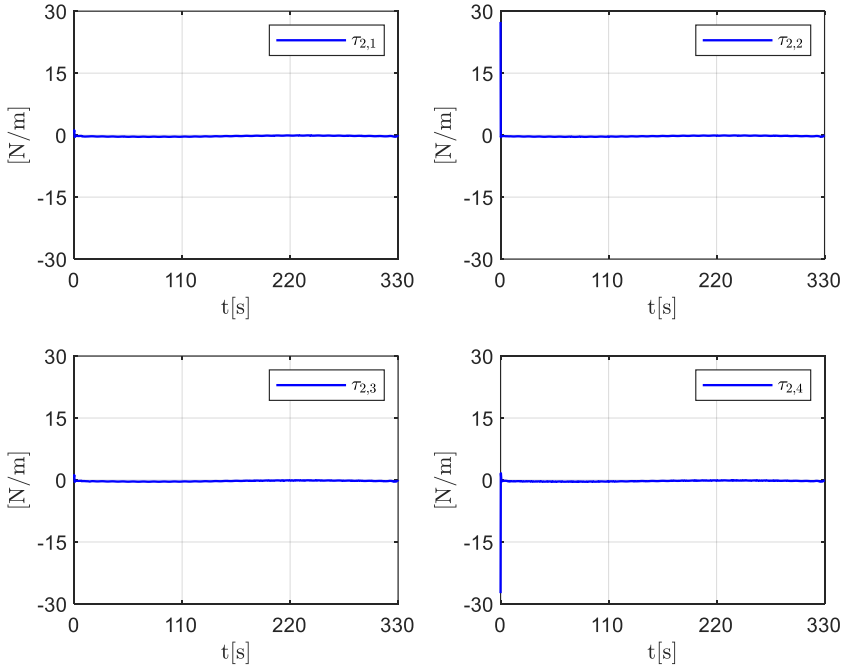


Figure 11. The moments of the followers.

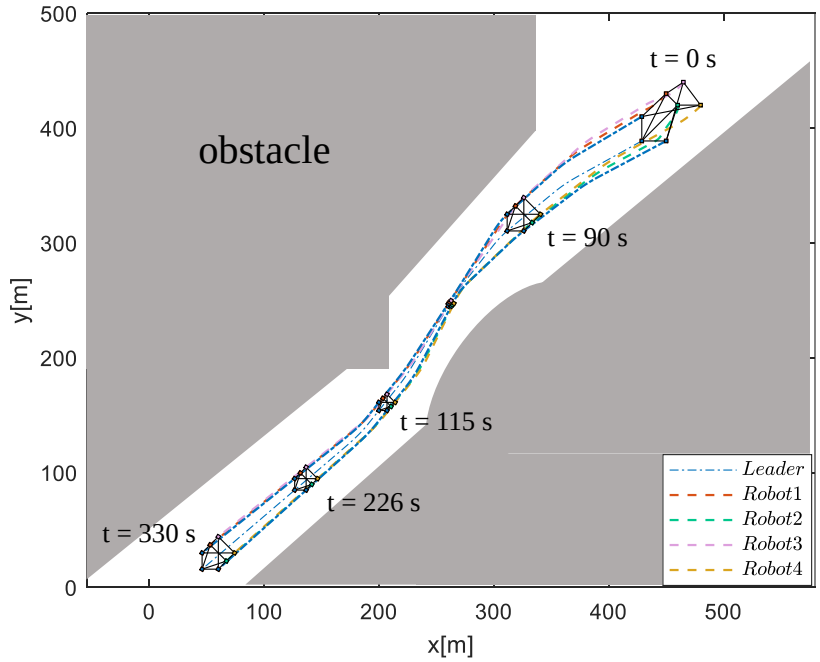


Figure 12. Formation motion trajectories in [4].

6. Conclusions

This paper investigates the time-varying formation control problem of robots considering model parameter uncertainties and external environmental disturbances, and it proposes an affine formation control method based on an Extended State Observer. The method is built upon a leader–follower formation structure and a graph theory-based formation framework. It includes both the principles for selecting leaders in the robot formation system and their trajectory planning methods as well as the design process of the disturbance-rejection affine formation controller for the followers. In this method, affine transformations and a stress matrix are introduced, allowing the formation system to perform formation transformations such as translation, rotation, scaling, and shearing without requiring each follower to know the corresponding target formation layout at all times. This improves the flexibility and adaptability of the formation system. To compensate for the effects of model parameter uncertainties and external environmental disturbances, this paper introduces an Extended State Observer design that considers the optimal solution of parameters and designs a disturbance-rejection affine formation controller. This enables the formation system to flexibly cope with complex and dynamic multi-robot monitoring environments, enhancing the system's robustness. Compared to existing time-varying formation control methods, the proposed control approach not only excels in adapting to uncertainties but also lays a foundation for further exploration and application in related fields.

Author Contributions: Conceptualization, J.Z.; methodology, H.W.; software, L.Z.; validation, K.L.; formal analysis, X.L.; investigation, Y.L.; resources, J.Z.; data curation, H.W.; writing—original draft preparation, J.Z. and H.W.; writing—review and editing, J.Z.; visualization, L.Z.; supervision, K.L.; project administration, X.L.; funding acquisition, J.Z. All authors have read and agreed to the published version of the manuscript.

Funding: This research received no external funding.

Data Availability Statement: Data is contained within the article.

Conflicts of Interest: The authors declare no conflict of interest.

References

1. Liu, Y.; Liu, J.; He, Z.; Li, Z.; Zhang, Q.; Ding, Z. A survey of multi-agent systems on distributed formation control. *Unmanned Syst.* **2024**, *12*, 913–926. [CrossRef]
2. Kamel, M.A.; Yu, X.; Zhang, Y. Formation control and coordination of multiple unmanned ground vehicles in normal and faulty situations: A review. *Annu. Rev. Control* **2020**, *49*, 128–144. [CrossRef]
3. Zelazo, D.; Giordano, P.R.; Franchi, A. Bearing-only formation control using an SE (2) rigidity theory. In Proceedings of the 2015 54th IEEEs Conference on Decision and Control (CDC), Osaka, Japan, 15–18 December 2015; pp. 6121–6126.
4. Liu, Y.; Lin, X. Formation scaling control for multiple unmanned surface vessels. In Proceedings of the OCEANS 2023-Limerick, Limerick, Ireland, 5–8 June 2023; pp. 1–5.
5. Alfakih, A.Y.; Taheri, N.; Ye, Y. On stress matrices of (d + 1)-lateration frameworks in general position. *Math. Program.* **2013**, *137*, 1–17. [CrossRef]
6. Lawton JR, T.; Beard, R.W.; Young, B.J. A decentralized approach to formation maneuvers. *IEEE Trans. Robot. Autom.* **2003**, *19*, 933–941. [CrossRef]
7. Alfakih, A.Y.; Ye, Y. On affine motions and bar frameworks in general position. *Linear Algebra Its Appl.* **2013**, *438*, 31–36. [CrossRef]
8. Das, A.K.; Fierro, R.; Kumar, V.; Ostrowski, J.P.; Spletzer, J.; Taylor, C.J. A vision-based formation control framework. *IEEE Trans. Robot. Autom.* **2002**, *18*, 813–825. [CrossRef]
9. Lin, Z.; Wang, L.; Chen, Z.; Fu, M.; Han, Z. Necessary and sufficient graphical conditions for affine formation control. *IEEE Trans. Autom. Control* **2015**, *61*, 2877–2891. [CrossRef]
10. Zhao, S. Affine formation maneuver control of multiagent systems. *IEEE Trans. Autom. Control* **2018**, *63*, 4140–4155. [CrossRef]
11. Pang, W.; Zhu, D.; Liu, C.; Wang, L. The multi-AUV time-varying formation reconfiguration control based on rigid-graph theory and affine transformation. *Ocean Eng.* **2023**, *270*, 113521. [CrossRef]
12. Chen, Y.W.; Chiang, M.L.; Fu, L.C. Three-dimensional maneuver control of multiagent systems with constrained input. *IEEE Trans. Cybern.* **2022**, *53*, 6133–6145. [CrossRef] [PubMed]
13. Zhu, C.; Huang, B.; Lu, Y.; Li, X.; Su, Y. Distributed affine formation maneuver control of autonomous surface vehicles with event-triggered data transmission mechanism. *IEEE Trans. Control Syst. Technol.* **2022**, *31*, 1006–1017. [CrossRef]
14. Pang, W.; Zhu, D.; Chu, Z.; Chen, Q. Distributed adaptive formation reconfiguration control for multiple AUVs based on affine transformation in three-dimensional ocean environments. *IEEE Trans. Veh. Technol.* **2023**, *72*, 7338–7350. [CrossRef]
15. Chen, L.; Sun, Z.; Li, C.; Zhu, B.; Wang, C. Satellite affine formation flying with obstacle avoidance. *Proc. Inst. Mech. Eng. Part G J. Aerosp. Eng.* **2019**, *233*, 5992–6004. [CrossRef]
16. Onuoha, O.; Tnunay, H.; Li, Z.; Ding, Z. Affine formation algorithms and implementation based on triple-integrator dynamics. *Unmanned Syst.* **2019**, *7*, 33–45. [CrossRef]
17. Xu, Y.; Li, D.; Luo, D.; You, Y.; Duan, H. Two-layer distributed hybrid affine formation control of networked Euler–Lagrange systems. *J. Frankl. Inst.* **2019**, *356*, 2172–2197. [CrossRef]
18. Chen, L.; Mei, J.; Li, C.; Ma, G. Distributed leader–follower affine formation maneuver control for high-order multiagent systems. *IEEE Trans. Autom. Control* **2020**, *65*, 4941–4948. [CrossRef]
19. Onuoha, O.; Tnunay, H.; Wang, C.; Ding, Z. Fully distributed affine formation control of general linear systems with uncertainty. *J. Frankl. Inst.* **2020**, *357*, 12143–12162. [CrossRef]
20. Luo, Z.; Zhang, P.; Ding, X.; Tang, Z.; Wang, C.; Wang, J. Adaptive affine formation maneuver control of second-order multi-agent systems with disturbances. In Proceedings of the 2020 16th International Conference on Control, Automation, Robotics and Vision (ICARCV), Shenzhen, China, 13–15 December 2020; pp. 1071–1076.
21. Li, D.; Cao, K.; Kong, L.; Yu, H. Fully distributed cooperative circumnavigation of networked unmanned aerial vehicles. *IEEE/ASME Trans. Mechatron.* **2021**, *26*, 709–718. [CrossRef]
22. Cui, J.; Liu, Y.; Nallanathan, A. Multi-agent reinforcement learning-based resource allocation for UAV networks. *IEEE Trans. Wirel. Commun.* **2019**, *19*, 729–743. [CrossRef]
23. Ning, Z.; Xie, L. A survey on multi-agent reinforcement learning and its application. *J. Autom. Intell.* **2024**, *3*, 73–91. [CrossRef]
24. Bai, C.; Yan, P.; Pan, W.; Guo, J. Learning-based multi-robot formation control with obstacle avoidance. *IEEE Trans. Intell. Transp. Syst.* **2021**, *23*, 11811–11822. [CrossRef]
25. Wang, H.; Li, N.; Wang, Y.; Su, B. Backstepping sliding mode trajectory tracking via extended state observer for quadrotors with wind disturbance. *Int. J. Control Autom. Syst.* **2021**, *19*, 3273–3284. [CrossRef]
26. Li, X.; Qi, G.; Guo, X.; Chen, Z.; Zhao, X. Improved high order differential feedback control of quadrotor UAV based on improved extended state observer. *J. Frankl. Inst.* **2022**, *359*, 4233–4259. [CrossRef]
27. Chen, L.; Liu, Z.; Dang, Q.; Zhao, W.; Wang, G. Robust trajectory tracking control for a quadrotor using recursive sliding mode control and nonlinear extended state observer. *Aerosp. Sci. Technol.* **2022**, *128*, 107749. [CrossRef]
28. Chwa, D. Tracking control of differential-drive wheeled mobile robots using a backstepping-like feedback linearization. *IEEE Trans. Syst. Man Cybern.-Part A Syst. Hum.* **2010**, *40*, 1285–1295. [CrossRef]

Disclaimer/Publisher's Note: The statements, opinions and data contained in all publications are solely those of the individual author(s) and contributor(s) and not of MDPI and/or the editor(s). MDPI and/or the editor(s) disclaim responsibility for any injury to people or property resulting from any ideas, methods, instructions or products referred to in the content.